ChemComm

Mechanism investigation of enhanced oxygen storage performance of $YBaCo_4O_{7+\delta}$ synthesized by glycine-complex decomposition method

Journal:	*ChemComm*
Manuscript ID	CC-COM-11-2021-006157.R2
Article Type:	Communication

COMMUNICATION

Mechanism investigation of enhanced oxygen storage performance of $YBaCo_4O_{7+\delta}$ synthesized by glycine-complex decomposition method

Received 00th January 20xx,
Accepted 00th January 20xx

DOI: 10.1039/x0xx00000x

Ting Ru Chen, [a] Takuya Hasegawa, [a] Sung Hun Cho, [b] Tomoyo Goto, [b] Tohru Sekino, [b] Masato Kakihana, [b] and Shu Yin *[a]

$YBaCo_4O_7$ oxygen storage material has been synthesized by the glycine-complex decomposition method at a low temperature of 800 ℃ and investigated from the crystal structure and reaction kinetics. This sample showed the highest storage/release speed among all the reported $YBaCo_4O_{7+\delta}$ materials

Oxygen storage materials (OSMs) have increased attention due to their wide practical application to oxygen-related technologies and their contribution to energy generations and environmental protection.[1-5] Recently, cobalt oxide $YBaCo_4O_{7+\delta}$ has become a research hotspot due to its outstanding oxygen storage/release capacity.[6-8] The crystal structure of $YBaCo_4O_{7+\delta}$ consists of two kinds of corner-sharing CoO_4 tetrahedrons in a ratio of 3:1. Triangular and Kagomé lattices of cobalt atoms are alternate stacking with each other and distinguished by different bond lengths as shown in Fig. 1b.[9,10] This compound was initially synthesized by the solid-state reaction method in 2002.[11] This material has been investigated mainly from the viewpoint of magnetic features.[12-15] Motohashi's group first reported that $YBaCo_4O_{7+\delta}$, synthesized by EDTA complex gel method, can adsorb and desorb oxygen up to $\delta \approx 1.5$ in a narrow temperature below 400 ℃, and further utilized Al-doped Co site to improve the thermal stability.[16-19] In addition, Parkkima also investigated various elements doped in different positions of $YBaCo_4O_{7+\delta}$ to enhance the phase stability.[10] However, it is noteworthy that the previous research only focused on modifying the synthesis process and tried to improve the oxygen storage performances and thermal stability by metal ions substitution in different sites. Moreover, all the reported sample exhibited poor kinetics during oxygen storage process. For the oxygen storage process mechanism and the impact of the particle size, structure on the oxygen intake/release speed during the TG measurement are still unclear, which may be more critical for developing advanced OSMs.

This work successfully synthesized two kinds of $YBaCo_4O_{7+\delta}$ products prepared by the glycine-complex decomposition method at 800 (YBCO-800) and 950 ℃ (YBCO-950). In order to investigate the mechanism for the enhanced oxygen intake/release speed and the low temperature synthesized sample exhibits superior oxygen storage performance in the air atmosphere. The in-situ observation of structure changes during the oxygen storage process, particle morphology, and oxygen intake/release behaviors of thus as-prepared compounds was comprehensively investigated. The selected-area electron diffraction (SAED) technique was performed to observe different local structures for these two samples, and this unique local structure makes $YBaCo_4O_7$, synthesized at low calcination temperature, possessed outstanding oxygen storage properties. Moreover, SEM, XPS, and XAFS results indicated that the low-temperature sample has a large specific surface area and contains many oxygen species, providing many active sites during the oxygen intake/release process and enhancing the interaction between the particle surface and gas molecules. This product still exhibited superior oxygen storage performance in the air atmosphere due to its stable structure, confirmed by in-situ high-temperature XRD results.

The crystal phase of the as-prepared $YBaCo_4O_{7+\delta}$ samples was determined by X-ray diffraction (XRD), as shown in Fig. 1a. The as-synthesized products are essentially the single phase of the oxygen-deficient $YBaCo_4O_7$ phase. Compared with the 950 ℃ sample, the (103) peak of the 800 ℃ sample revealed a slight difference. The crystal structure of $YBaCo_4O_7$ was refined by Rietveld analysis using the XRD profile and the Rietan-FP program (Fig. S1),[20] which gave good R and S values, as listed in Table S1, by indexing the P63mc space group of the layered structure. (As illustrated in Fig. 1b using the VESTA program[21]). The refined crystallographic and atomic parameters are also summarized in Table S2.

[a] *Institute of Multidisciplinary Research for Advanced Material (IMRAM), Tohoku University, Sendai, Miyagi, Japan 980-8577.*
[b] *The Institute of Scientific and Industrial Research, Osaka University, 8-1, Mihogaoka, Ibaraki, Osaka 567-0047, Japan.*
†Electronic Supplementary Information (ESI) available: See DOI: 10.1039/x0xx00000x

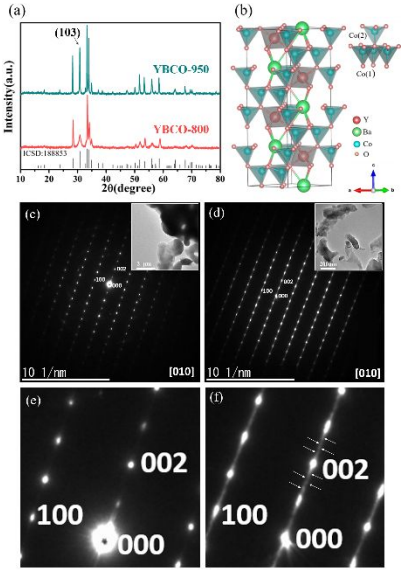

Fig. 1 (a) XRD patterns of $YBaCo_4O_{7+\delta}$ synthesized at different calcination temperatures. (b) The standard model structure of $YBaCo_4O_7$. The [010]-incidence ED patterns of (c) 950 ℃ sample and (d) 800 ℃ sample. Enlarged ED patterns of (e) 950 ℃ sample and (f) 800 ℃ sample.

According to the XRD refinement results, the 800 ℃ sample shows a larger c value than that of the 950 ℃ sample. This difference suggests that the structure of the 800 ℃ sample might have slightly changed during the calcination process. The XPS spectra of Co 2p and O 1s before TG measurement were carried out to investigate the oxidation state of these two samples, as shown in Fig. S2. The B.E. (binding energies) and atomic surface ratios are also presented in Table S3 and Table S4. The higher Co^{3+}/Co^{2+} ratio of 800 ℃ sample than 950 ℃ sample was confirmed by XPS results, as well as the largest adsorbed oxygen (OA) onto the surface of 800 ℃ sample, which indicates that the 800 ℃ sample possesses much extra oxygen and high cobalt valance state. We also calculated the actual oxygen content of these two samples before TG measurement by iodometric titration from three parallel analyses.[22] We confirmed the exact oxygen content of these two samples (Table S3). In this case, the 800 ℃ sample possessed the high oxygen content in the structure, demonstrating the higher valence of cobalt in the 800 ℃ sample, consistent with XPS results. This result was further demonstrated by the X-ray adsorption fine structure (XAFS) of the $YBaCo_4O_7$ sample before TG measurement, as shown in Fig. S3. The adsorption edge of the 800 ℃ sample is located at higher photon energy than the 950 ℃ sample before TG measurement, indicating that the higher valence of cobalt in the 800 ℃ sample. Moreover, the Co K-edge EXAFS oscillations of the 800 ℃ sample before the TG test (Fig. S3c) shows a significant difference compared with the 950℃ sample in the range of 6-10 $Å^{-1}$, which further demonstrates the different local structure and local atomic arrangements of the low-temperature sample.

The microstructures and morphologies of $YBaCo_4O_7$ were further observed by SEM and TEM (Fig. 1 and Fig. S4). The average size of the primary particles, ~300 nm for the 800 ℃ sample, is much smaller than that for the 950 ℃ sample (~2 μm). The specific surface area of the 800 ℃ sample was 7.7 m^2/g, while the 950 ℃ sample was 3.1 m^2/g, respectively, which was confirmed with the N_2 adsorption isotherms, as shown in Fig. S5. Improving the specific surface area is beneficial for improving the number of active sites in the oxygen storage/release process. TEM images can clearly observe the nanoparticles of the 800 ℃ sample (Fig. 1d insert picture). Moreover, SAED has been employed for the in-depth characterization of sample structure. Fig. 1c-d shows two ED patterns were taken with the incident electron beam parallel to the [010] zone axes of the two samples, which indicated a typical diffraction pattern of a $YBaCo_4O_7$ hexagonal lattice.[23] The 950℃ sample was observed to have no super-lattice patterns along the [010] axis, as shown in the enlarged pattern of the 950℃ sample (Fig. 1e). However, obviously super-lattice patterns were observed in the low-temperature sample (Fig. 1f), as indicated by the arrows. This result further demonstrated that the structure of the low-temperature sample has changed, which might be ascribed to the stacking faults in the crystal structure, resulting in a super-lattice structure during calcination at low temperature in the N_2 atmosphere. This unique structure would positively affect the structure change during the oxygen storage/release process.

TG curves were recorded to determine the oxygen adsorption/desorption behavior of $YBaCo_4O_{7+\delta}$, as depicted in Fig. S6. The designed condition was to heat the sample to 500 ℃ in an O_2 atmosphere with a heating rate of 1 ℃/min and then cooled the sample back to room temperature at the same rate. The 950 ℃ sample showed a maximum oxygen storage capacity of 3.2 wt.%. However, the 800 ℃ sample only revealed a maximum OSC of 2.4 wt.%, which can be ascribed to the different oxygen content in these two materials according to the iodometric titration results (Table S3). The XPS results of these two samples after TG measurement are depicted in Fig. S2. The Co^{3+}/Co^{2+} ratio of the 950 ℃ sample is slightly higher than the 800 ℃ sample after TG measurement, which suggests that the valence of the 950 sample has a significant change during the oxygen intake/release process, resulting in a high oxygen storage capacity. Isothermal oxygen storage/release behaviors were also carried out to measure the oxygen adsorption/desorption speed of $YBaCo_4O_{7+\delta}$ at different operating temperatures (350, 360 and 370 ℃) (Fig. S7). The 800 ℃ sample showed outstanding kinetic performance of the oxygen adsorption/desorption process at operating temperatures 350 and 360 ℃. The time required for complete oxygen store/release is 5/6 min at 350 ℃ and 5/4 min at 360 ℃, respectively (Fig. S8a-b). In comparison, the 950 ℃ sample takes longer to complete the storage and release of oxygen (Fig. S8c-d). In addition, the 800℃ sample showed the highest intake/release speed among all the $YBaCo_4O_{7+\delta}$ materials reported to date as summarized in Table S5, to the best of our knowledge. This result demonstrated that the small particles, comparatively large specific surface area, and unique local structure of 800 ℃ sample positively impact the oxygen intake/release performances, especially the oxygen storage/release rate.

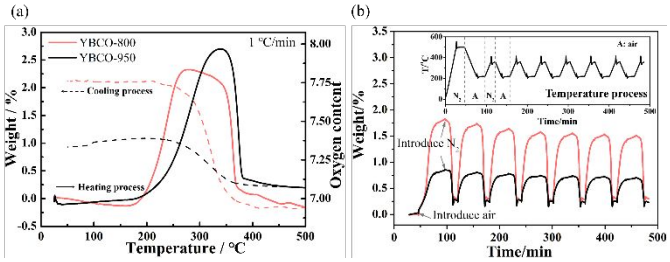

Fig. 2. (a) TG curves of $YBaCo_4O_{7+\delta}$ in the air atmosphere from 30 ℃ to 500 °C with heating/cooling rates of 1 °C/min for 800 and 950 ℃ samples. (b) TG curves of $YBaCo_4O_{7+\delta}$ measured by TSA processes during swing between 220 and 360 ℃. N_2 is the reducing gas, air is the oxidizing gas. (insert picture: temperature process)

In order to demonstrate the practical application of $YBaCo_4O_{7+\delta}$, the oxygen intake/release processes in the air atmosphere were also carried out, as shown in Fig. 2. The 800 ℃ sample showed a high oxygen storage capacity of around 2.32 wt.% in the heating process, which is similar to the result in the oxygen atmosphere (Fig. S6). Moreover, this sample could still maintain OSC of 2.11 wt.% after cooling to room temperature, while the 950 ℃ sample showed a maximum OSC of 2.70 wt.% in the heating process but only exhibited oxygen storage capacity of 1.0 wt.% during the cooling process. In addition, we further investigated the oxygen intake/release processes in the simple air (only 21% O_2 and 79% N_2) atmosphere, as depicted in Fig. S9. The oxygen storage capacity and the adsorbed oxygen temperature range sharply decreased due to changes in oxygen partial pressure. As for the 800 ℃ sample, it shows excellent oxygen storage performance in both oxygen and air atmosphere, suggesting that oxygen pressure and carbon dioxide in the air have only a tiny effect on the oxygen storage property, which could be ascribed to the small particles, comparatively large specific surface area, and the unique super-lattice structure of the low-temperature sample. In addition, a temperature swing adsorption process was also performed to investigate the oxygen storage/release performance, as shown in insert picture (Fig. 2b). The sample is heated to 500 ℃ under a nitrogen atmosphere and then cooled to 220 ℃ in airflow maintained 20min (oxygen storage process), subsequently heated to 360 ℃ in N_2 gas flow maintained 10 min (oxygen release process), the test is repeated 7 cycles, the temperature process as presented in Fig. 2b. It is worth noting that the 800 ℃ sample reveals a higher oxygen storage capacity than that of the 950 ℃ sample during the TSA process in the air atmosphere. In addition, the long cycle performance of the 800℃ sample measured by the TSA process is also revealed in Fig. S10. These results further demonstrate that $YBaCo_4O_{7+\delta}$ synthesized at low temperature possessed a promising practical application.

In order to investigate the structural change during the oxygen intake/release process, in-situ high-temperature XRD was carried out, as shown in Fig. 3. For the high-temperature XRD (HT-XRD), measurements were carried out in a static air atmosphere at a temperature range of 30−500 °C with a heating rate of 10 °C /min. The corresponding TG curves are presented in Fig. S11. There is no apparent structural change in the low-temperature range for the 950 °C sample, as shown in area (I). As temperature increases, the changes take place at 240 °C. It is

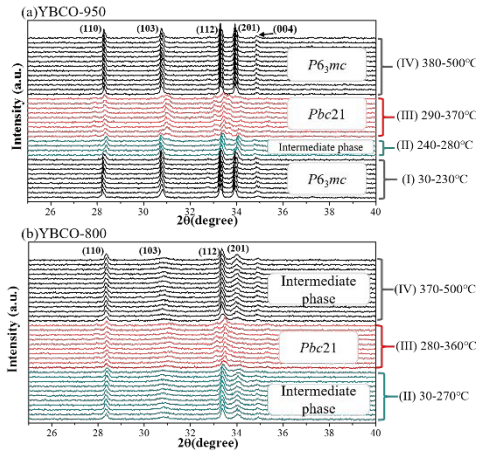

Fig. 3. In-situ high temperature XRD results of $YBaCo_4O_{7+\delta}$ in 2θ of 25-40°. (a) 950 °C sample from 30 to 500 °C heating at air atmosphere including four areas. (b) 800 °C sample from 30 to 500 °C heating in the air atmosphere including three areas.

worth noting that (110), (112), and (201) peaks start to shift to a higher angle, as shown in Fig. 3a (area II). This could be attributed to the heat treatment inducing a cell expansion to adapt to the change from CoO_4 tetrahedron to CoO_6 octahedron during the oxygen storage process (intermediate phase). As temperature continuous to elevate, some prominent peaks disappeared and new peaks appeared at 290 °C (area III), corresponding with previous research,[24] which can be ascribed to the structural phase transition of oxygen-depleted $YBaCo_4O_7$ with $P6_3mc$ space group to oxygen-rich $YBaCo_4O_{7+\delta}$ with $Pbc21$ space group during oxygen adsorbed process.[25] When the temperature increases, the diffraction pattern returns to the initial phase at 380 °C and maintains to 500 °C (area IV). However, for the 800 °C sample, there is no obvious structural change in the range of 30-270 °C, as shown in Fig. 3b. The clear difference between these two samples was depicted in the enlarged patterns (Fig. S12). In addition, we summarized the main peak positions of these two samples at the room temperature and 240 ℃ in Table S6, respectively. We can find that three main peaks (110), (112) and (201) of 950 ℃ sample shift to a higher angle and their peak positions are almost the same as those of 800 ℃ sample at 240℃. This result indicated that crystal phase of 800 ℃ is the same as the intermediate phase which formed during the heating process of 950 ℃ sample. The diagram of structural changes during oxygen storage process are as shown in Fig. S13.

The oxygen adsorption/desorption reaction process of $YBaCo_4O_{7+\delta}$ sample is a typical gas-solid reaction, involving complicated heat and mass transfer processes. In the presence of oxygen, a series of transformations on the oxide catalyst surface occurs according to the previous reported formula:[26,27]

$$O_2 \rightleftharpoons \underline{O_2} \rightarrow \underline{O_2^-} \rightarrow \underline{O_2^{2-}} \rightarrow \underline{2O^{2-}} \rightarrow 2O^{2-}$$

The underlines represent the chemisorbed or surface species. It can be speculated that the oxygen intake/release processes of $YBaCo_4O_{7+\delta}$ proceed with the following three steps: Firstly, adsorbed O_2 molecules from gas flow; Next, some adsorbed oxygen molecules obtained the electrons, and different adsorbed oxygen species are formed (O^{2-}, O_2^{2-}), gradually enriched with electrons until the state of O^{2-} is reached. Finally, these adsorbed O^{2-} ions eventually migrated into the structure

to form the lattice oxygen. For the $YBaCo_4O_7$ structure, the CoO_4 tetrahedron will change to the CoO_6 octahedron and the space

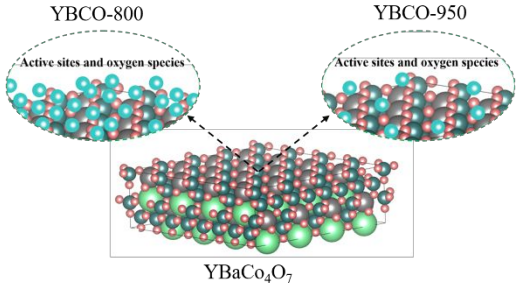

Fig. 4 A simple surface mechanism images of these two samples during adsorbed oxygen process.

group will change from $P6_3mc$ to $Pbc21$, as described in the In-situ high-temperature XRD results. The 800 ℃ sample revealed small particles and large specific surface area, which is beneficial for improving the number of active sites in the oxygen storage/release process. These active sites could adsorb more oxygen molecules and quickly change to the O^{2-} ions. Moreover, the adsorbed O^{2-} ions migrated into the structure to form the lattice oxygen. In-situ XRD results and Fig. S13 indicated the 800 ℃ sample revealed an intermediate phase, which can complete the phase transition faster and easier than that of the 950℃ sample during the oxygen storage process. This intermediate phase may be more conducive to the diffusion of O^{2-} and the reversible conversion from CoO_4 tetrahedron to CoO_6 octahedron, resulting in 800 ℃ sample exhibited outstanding oxygen storage/release speed.

In summary, $YBaCo_4O_{7+\delta}$ was successfully synthesized by the glycine-complex decomposition method at 800 ℃and 950℃ and comprehensively investigated the oxygen storage/release behaviors. The preparation of 800 ℃ sample revealed outstanding oxygen storage performance. The oxygen intake process at 350 and 360 ℃ is fast and completed only within 5 min. The time required for the complete oxygen release process is 6 and 4 min, respectively. This can be attributed to its unique local structure, large specific surface area, small particle sizes, and relatively stable structure during the oxygen adsorption process. In addition, the temperature swing adsorption process further demonstrates the promising application potential of the low-temperature synthesized $YBaCo_4O_{7+\delta}$. The present work explained the mechanism of enhanced oxygen storage performance of low-temperature sample and introduced a new insight for the low-temperature synthesis of new oxygen storage materials.

This research was supported by Council for Science, Technology and Innovation (CSTI), Cross-ministerial Strategic Innovation Promotion Program (SIP), “Energy systems toward a decarbonized society” (Funding agency: JST), and was also partly supported by the JSPS Grant-in-Aid for Scientific Research (20H00297), Grant-in-Aid for Scientific Research on Innovative Areas “Mixed anion” (No. 16H06439), and also by the Dynamic Alliance for Open In-novation Bridging Human, Environment and Materials in Network Joint Research Center for Materials and Devices. "The XAFS measurements were performed with the BL12C at the Photon Factory (PF) with the approval of the High Energy Accelerator Research Organization (KEK) (Proposal No. 2020P001). We also thank professor Teruki Motohashi for his help in this research. Also T.Ru CHEN thanks the China Scholarship Council for providing the scholarship.

There are no conflicts to declare.

References

1 D. T. Augusto, M. Gianluca, O. Angelo, P. Stefano, R. Federico and R. Vincenzo, *Ind. Eng. Chem. Res*., 2021, 18, 6653–6661.
2 D. W. Zeng, Y. Qiu, M. Li, L. Ma, D. X. Cui, S. Zhang and R. Xiao, *Appl. Catal. B*, 2021, 281, 119472.
3 A. Klimkowicz, T. Hashizume, K. Cichy, S. Tamura, K. Swierczek, A. Takasaki, T. Motohashi and B. Dabrowski, *J. Mater. Sci.,* 2020, 55, 15653–15666.
4 C. W. Sun, J. A. Alonso and J. J. Bian, *Adv. Energy Mater.,* 2021, 11, 2000459.
5 Z. Y. Zhou, P. H. Michael and D. Luss, *Catal. Today*., 2021, 360, 375-387.
6 M. Xu, I. Ermanoski, E. B. Stechel and S. Deng, *Chem. Eng. J.*, 2020, 389, 124026.
7 L. Hou, Q. B. Yu, T. Wang, K. Wang, Q. Qin and Z. F. Qi, *Korean J Chem Eng,* 2018, 35, 626–636.
8 D. S. Tsvetkov, P. S. Maram, N. S. Tsvetkova, A. Y. Zuev and A. J. Navrotsky, *Phys. Chem. A*, 2018, 122, 9597–9604.
9 O. Parkkima and M. Karppinen, *Eur. J. Inorg. Chem*., 2014, 2014, 4056-4067.
10 O. Parkkima, H. Yamauchi and M. Karppinen, *Chem. Mater.*, 2013, 25, 599-604.
11 M. Valldor and M. Andersson, *Solid State Sci.*, 2002, 7, 923-931.
12 M. Soda, S. Itoh, T. Yokoo, G. Ehlers, K. F. Hazuki and T. Masuda, *Phys. Rev. B,* 2020, 101, 214444.
13 A. K. Bera, S. M. Yusuf and S. Banerjee, *Solid State Sci*., 2013, 16, 57-64.
14 P. Manuel, L. C. Chapon, P. G. Radaelli, H. Zheng and J. F. Mitchell, *Phys. Rev. Lett.*, 2009, 103, 037202.
15 L. C. Chapon, P. G. Radaelli, H. Zheng and J. F. Mitchell, *Phys. Rev. B,* 2006, 74, 172401.
16 M. Karppinen, H. Yamauchi, S. Otani, T. Fujita, T. Motohashi, Y. H. Huang, M. Valkeapaa and H. Fjellvag, *Chem. Mater*., 2006, 18, 490-494.
17 T. Motohashi, S. Kadota, H. Fjellvag, M. Karppinen and H. Yamauchi, *Mater. Sci. Eng. B,* 2008, 148, 196–198.
18 T. Komiyama, T. Motohashi, Y. Masubuchi and S. Kikkawa, *Mater. Res. Bull.*, 2010, 10, 1527-1532.
19 S. Räsänen, T. Motohashi, H. Yamauchi and M. J. Karppinen, *Solid State Chem.*, 2010, 183, 692-695.
20 F. Izumi and K. Momma, *Solid State Phenom*., 2007, 130, 15–20.
21 K. Momma and F. J. Izumi, *Appl. Crystallogr*., 2008, 41, 653-658.
22 M. Karppinen, M. Matvejeff, K. K. Saloma and H J. Yamauchi, *Mater. Chem*., 2002, 12, 1761-1764.
23 M. A. Kirsanova, V. D. Okatenko, D. A. Aksyonov, R. P. Forslund, J. T. Mefford, K. J. Stevenson and A. M. Abakumov, *J. Mater. Chem. A*, 2019, 7, 330-341.
24 V. Markus, M. Karppinen, T. Motohashi, R. S. Liu, J. M. Chen and H. Yamauchi, *Chemistry Letters*., 2007, 36, 1368-1369.
25 O. Chmaissem, H. Zheng, A. Huq, P. W. Stephens and J. F. Mitchell, *J Solid State Chem,* 2008,181, 664–672.
26 N. A. Merino, B. P. Barbero, P. Eloy and L. E. Cadu´s, *Appl. Surf. Sci*., 2006, 253, 1489–1493.
27 H. He, H. X. Dai and C. T. Au, *Catal. Today*., 2004, 90, 245-254